Horizon Measures: A Novel View-Independent Shape Descriptor

Eugene Zhang* Oregon State University
Vivek Jadye† MathWorks
Christine Escher‡ Oregon State University
Peter Wonka§ King Abdullah University of Science and Technology
Yue Zhang¶ Oregon State University
Xiaofei Gao‖ Oregon State University

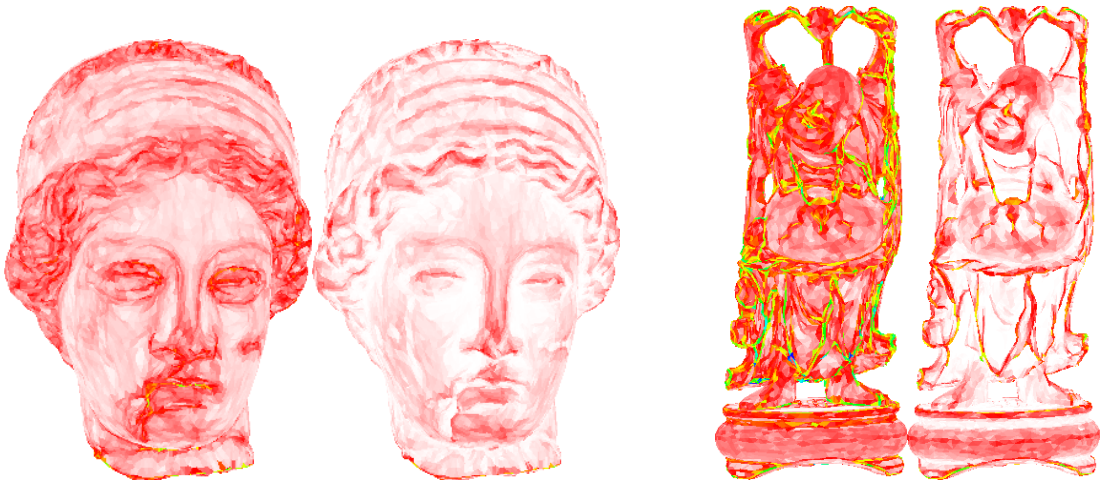

(a) (b) (c) (d)

Figure 1: *We introduce two shape descriptors, the horizon measure (a, c) and the visible horizon measure (b, d), which describe the respective likelihood of contours and visible contours in a region in the surface. Red indicates relatively high horizon and visible horizon measures, while white indicates relatively low measures. The visible horizon measure is always less than the horizon measure.*

Abstract

In this paper we seek to answer the following questions: where do contour lines and visible contour lines (silhouette) tend to occur in a 3D surface. Our study leads to two novel shape descriptors, the horizon measure and the visible horizon measure, which we apply to the visualization of 3D shapes including archeological artifacts. In addition to introducing the shape descriptors, we also provide a closed-form formula for the horizon measure based on classical spherical geometry. To compute the visible horizon measure, which depends on the exact computation of the surface visibility function, we instead of provide an image-based approach which can process a model with high complexity within a few minutes.

Keywords: horizon measure, shape descriptors, NPR, digital geometry processing

Concepts: •**Computing methodologies** → **Shape modeling;**

*e-mail:zhange@eecs.oregonstate.edu
†e-mail:vikikishor@gmail.com
‡email:tine@science.oregonstate.edu
§email:pwonka@gmail.com
¶e-mail:zhangyue@oregonstate.edu
‖e-mail:gaoxia@onid.oregonstate.edu

SA '16 Technical Briefs ,, December 05-08, 2016, , Macao

1 Introduction

Line drawing is a fascinating form of art that has inspired many generations of artists. Recently, there has been much work in using computers to generate images that simulate line art from a 3D surface. One of the main challenges is to compute the feature lines given the shape and viewpoint. There are two classes of approaches, both of which draw the *silhouette* as well as additional lines. In the first approach, the additional lines are *view-dependent*, i.e., they change when the viewpoint changes and thus need to be computed on the fly. Examples include suggestive contours [DeCarlo et al. 2003] and apparent ridges [Judd et al. 2007]. The second approach extracts feature lines that are *view-independent*, such as ridge and valley lines [Ohtake et al. 2004], as well as demarcating curves [Kolomenkin et al. 2008]. Cole et al. [2012] perform user studies on where artists tend to draw lines given an input 3D shape.

In this paper, we ask the following fundamental question: where do contour lines tend to occur in a 3D shape? More precisely, what is the probability of a point on the surface to be on the contour (or silhouette) given all possible viewing directions. While contour lines are view-dependent, this likelihood is *view-independent* and can provide insight into the geometric structure of the surface.

In answering this question, we introduce two new shape descriptors. The first descriptor, the *horizon measure*, defined on each triangle in the mesh surface, is the likelihood of the triangle containing part of the *contours* over all possible exterior viewing directions. Recall that the contours are the boundaries between the forward-facing part of the surface and the backward-facing part of the surface. Not

ISBN: 978-1-4503-4541-5/16/12 $15.00
DOI: http://dx.doi.org/10.1145/3005358.3005390

all contours are visible, and the visible part is referred to as the silhouette. Our second feature definition, termed *visible horizon measure*, is the likelihood of a triangle in the mesh containing part of visible contours. Note that both the horizon measure and the visible horizon measure are view-independent. Figure 1 shows the horizon measure (left) and the visible horizon measure (right) for the Venus and Buddha models.

In addition, we provide efficient algorithms to compute both measures. For the horizon measure, we provide an analytical formula that allows the measure to be computed exactly and quickly. For the visible horizon measure, we develop an efficient approach based on the sampling of the space of viewing directions. We have applied our shape descriptors to the visualization of shapes, including archeological artifacts.

2 Horizon Measure

In this section we provide details on the horizon measure and the visible horizon measure. Given a surface $M \subset R^3$ and an orthographic viewing direction $w \in S^2$, a point $\mathbf{p} \in M$ is called *a horizon point* with respect to w if $w \cdot N(\mathbf{p}) = 0$, where $N(\mathbf{p})$ is the unit surface normal at point $\mathbf{p}$. The set of viewing directions for which $\mathbf{p}$ is a horizon point can be denoted by $H_\mathbf{p} = \{w \in S^2 \mid w \cdot N(\mathbf{p}) = 0\}$, which is a great circle as shown in Figure 2 (left). $H_\mathbf{p}$ is referred to as the *horizon viewer set* with respect to $\mathbf{p}$.

The concept of the horizon viewer set can be extended to a region in the surface as follows. Given a surface $M \subset R^3$ and a subset $K \subset M$, the *the horizon viewer set* for K is $H_K = \bigcup_{\mathbf{p}\in K} H_\mathbf{p}$, or equivalently $H_K = \{w \in S^2 \mid \exists \mathbf{p} \in K \text{ such that } N(\mathbf{p}) \cdot w = 0\}$.

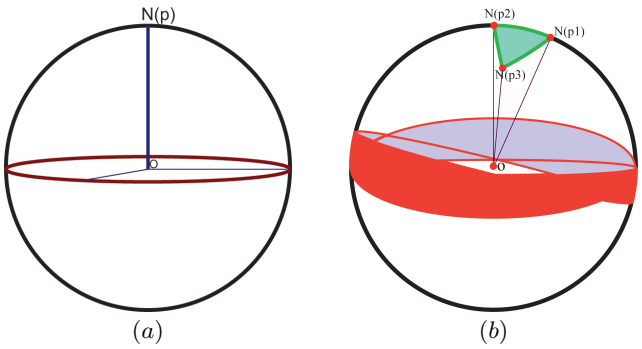

Figure 2: *Left: given a point **p** in the surface (not shown), the set of directions in the camera space (the sphere shown) from which **p** is considered as a horizon point is a great circle (shown in red) perpendicular to the normal $N(\boldsymbol{p})$. Right: he horizon viewer set (red stripe) for a triangle on surface (whose normal spans the green triangle in S^2).*

The area of the horizon view set H_K is a descriptor for K. The larger the area, the more likely K contains contours. We refer to this area as the *absolute horizon measure* of K and denote it by $h(K)$. We define the *relative horizon measure*, denoted by $\widehat{h}(K)$, as the ratio between $h(K)$ and the area of K. Furthermore, we define the horizon measure of a point $\mathbf{p} \in M$ as $\lim_{r\to 0} \widehat{h}(K_{\mathbf{p},r})$ where $K_{\mathbf{p},r} = \{\mathbf{q} \in M \mid \mathbf{dist}(\mathbf{q}, \mathbf{p}) \leq r\}$.

Note that the horizon measure is always non-negative. This is a sharp contrast to the *Gaussian curvature* and the *mean curvature*, both of which can be negative. In fact, it is interesting to note the dual relationship between the horizon measure and the absolute Gaussian curvature at a point. To see this we review the concept of

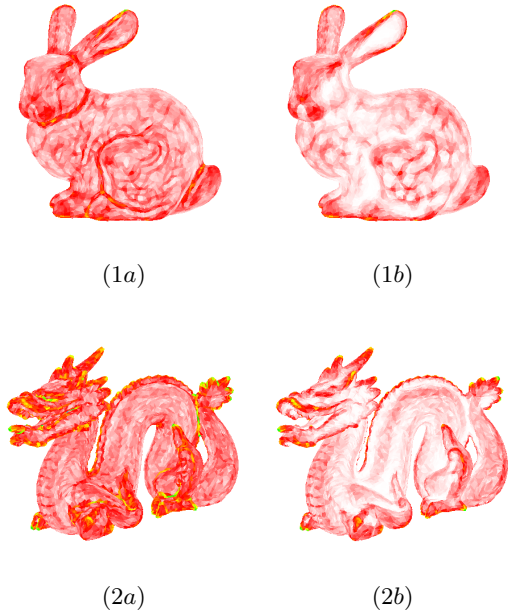

Figure 3: *This figure compares the horizon measure and the visible horizon measure with the bunny. Notice that the horizon measure is usually larger than the visible horizon measure. Moreover, the two measures tend to agree near ridge lines and disagree near valley lines and inverted region. For example, while the horizon measure is nearly constant on the bunny's ear, the visible horizon measure is significantly lower inside the ear than outside the ear. In addition, the horizon measure is high in the crease where the dragon's tail touches the body. In contrast, the visible horizon measure is low in that region. This is due to the fact the visible horizon measure takes into account the self occlusions.*

the *Gauss map*. The Gauss map for a surface M is $\Gamma : M \to S^2$ such that $\forall \mathbf{p} \in M, \Gamma(\mathbf{p}) = N(\mathbf{p})$.

Given $K \subset M$, the area of the set $\{N(\mathbf{p}) \mid \mathbf{p} \in M\}$ measures the variations of the normal in K. The Gaussian curvature of a point in M is defined as $\lim_{r\to 0} \frac{area(\Gamma(K_{\mathbf{p},r}))}{area(K_{\mathbf{p},r})}$ where $K_{\mathbf{p},r} = \{\mathbf{q} \in M \mid \mathbf{dist}(\mathbf{q}, \mathbf{p}) \leq r\}$. Note that $area(K_{\mathbf{p},r})$ refers to the signed area. By replacing the $area(\Gamma(K_{\mathbf{p},r}))$ with $area(H(K_{\mathbf{p},r}))$ (which is not signed), we obtain the definition for the horizon measure of $\mathbf{p}$.

Horizon Measure Computation on a Triangle Mesh: In computer graphics, a surface is often represented as a triangle mesh, with a set of vertices V, a set of edges E and a set of triangles F. The normal is assumed to be continuous across the surface. This is achieved by computing the normal at the vertices and linearly interpolating them for the points in the triangles. Under this assumption, we compute the horizon measure per triangle. This requires the evaluation of the area of the horizon viewer set corresponding to the triangle. Figure 2 (right) shows a spherical triangle (green) which corresponds to the normal variation over a triangle $\triangle p_1p_2p_3$ in a mesh surface. The red region near the equator is the horizon viewer set for $\triangle p_1p_2p_3$.

We now return to the horizon measure of a triangle in a mesh. The horizon measure of a triangle $\triangle U_1U_2U_3$ in a mesh surface M is $\frac{\sum_{i=1}^{3} \arccos(\Gamma(U_{i-1})\cdot\Gamma(U_{i+1}))}{2\pi}$. The proof is provided in the Appendix. Figure 1 shows the horizon measure computed on Venus and Buddha, while Figure 3 shows this for the bunny and the dragon.

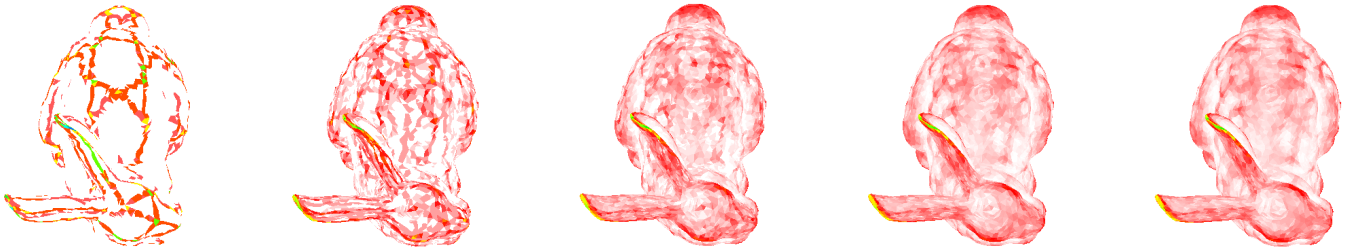

(a) (b) (c) (d) (e)

Figure 4: *The visible horizon measure on the bunny computed using five different camera systems. In (a), the cameras were placed at the vertices of an icosahedron. From (b)-(e), the cameras are placed on the vertices of a mesh obtained by performing Loop subdivision to the camera system used in the previous case. Notice that the accuracy increases with more cameras. The difference between (d) and (e) is very small.*

3 Visible Horizon Measure

The horizon measure provides information on where contour lines tend to occur. While this information is important to understand the structure of a surface, we note that in line drawing not all contour lines are visible from a given viewpoint. Invisible contour lines are mostly due to self-occlusions in the surface. When illustrating a surface, the *silhouette*, i.e. visible contour lines, are usually drawn. This immediately brings up the question where in the surface visible contours are more likely to occur. In this section, we introduce the notion of the *visible horizon measure* which encodes this information.

Given a surface $M \subset R^3$ and an orthographic viewing direction $w \in S^2$, a point $\mathbf{p} \in M$ is called *a visible horizon point* with respect to w if $\mathbf{p}$ is a horizon point with respect to w and is visible from w. The set of viewing directions for which $\mathbf{p}$ is a visible horizon point can be denoted by $H'_{\mathbf{p}}$ and is referred to as the *visible horizon viewer set* with respect to $\mathbf{p}$.

Similar to the horizon viewer set, the concept of the visible horizon viewer set can be extended to a region in the surface. Like the horizon measure, the visible horizon measure is always non-negative. It is worth noting that the visible horizon measure is always less than or equal to the horizon measure given a region in the surface. This follows from the fact that the visible horizon viewer set is necessarily a subset of the the horizon viewer set. In addition, the visible contours seem more likely to appear in convex regions in the surfaces. This means that the visible horizon measure tends to agree with the horizon measure in those regions. Figure 1 compares the two measures on the Venus model. Notice that the horizon measure (left) and the visible horizon measure are similar on the ridge of Venus's nose. In contrast, the two measures tend to differ significantly near concave regions, such as the sides of the nose and the lip lines. Figure 3 provides additional comparisons between the two measures with the bunny and dragon models.

Unfortunately, the visible horizon measure depends on the visibility function, which is a binary relationship between points on the mesh surfaces and points in the camera space. The visibility function lacks an analytical formula and can be discontinuous. This in turn makes the computation of the visible horizon measure more challenging. To address this issue, we employ the following image-based sampling approach, inspired by the approach of Zhang and Turk [2002] to compute the shape descriptor *surface visibility* that they introduce.

First, we select a set of evenly-spaced camera positions in the camera space. We only use orthographic cameras that are situated outside the bounding box of the input mesh. Under these conditions, the space of all possible camera locations form a sphere, which we tessellate into a triangle mesh. Second, from each vertex of the triangle mesh representing the camera space, we render the mesh using its silhouette. Unlike line art where the silhouette is rendered in a color (usually black) different from the background (usually white), we assign the color of each silhouette edge based on the triangle containing it. Every triangle is assigned a unique color. Note that the silhouette edges are extracted based on the method of Hertzmann and Zorin [2000], in which the dot product between the surface normal and the rays emanating from the eye is evaluated at the vertices of the input mesh. This dot product is then used to extract silhouette edges inside the faces of the triangle mesh. Next, from the same viewpoint, we scan the image generated from the previous step and increment the counter of each face in the triangle mesh whose unique color appears at least once in the aforementioned image. This indicates that at least some silhouette appears in such a triangle from this viewpoint. Once all the viewpoints have been processed, we compute for each triangle its visible horizon measure. This is approximated by the ratio between the number of camera positions from which some silhouette appeared inside the triangle and the total number of cameras.

The accuracy of this method largely depends on the number of camera directions used in the sampling stage. Figure 4 shows this with five different samplings of the camera space. Notice that the result converges as more sample camera directions are used. On the other hand, the more samples, the more computational cost is incurred. In practice, we have found that for our test models it is sufficient to use 644 cameras, representing the vertices on an icosahedron subdivided three times based on Loop subdivision. This provides a reasonable tradeoff between the accuracy and computational speed.

Performance: We have applied the horizon measure and visible horizon measure to a number of well-known data sets, such as the Stanford Bunny, Happy Buddha, Dragon, and Feline. In addition, we test our methods on a number of archeological data sets [Kolomenkin et al. 2008]. The performance data is collected from a computer with an Intel Xeon E3-1225 3.20 GHz processor, 16 GB of RAM, and an NVIDIA NVS 310 graphics card. The computational cost for each test case is mostly due to the computation of the visible horizon measure, which is dependent on the number of faces in the mesh as well as the number of vertices in the mesh tessellating the camera space. All the test cases require at most two minutes of computation time, including the archeological models

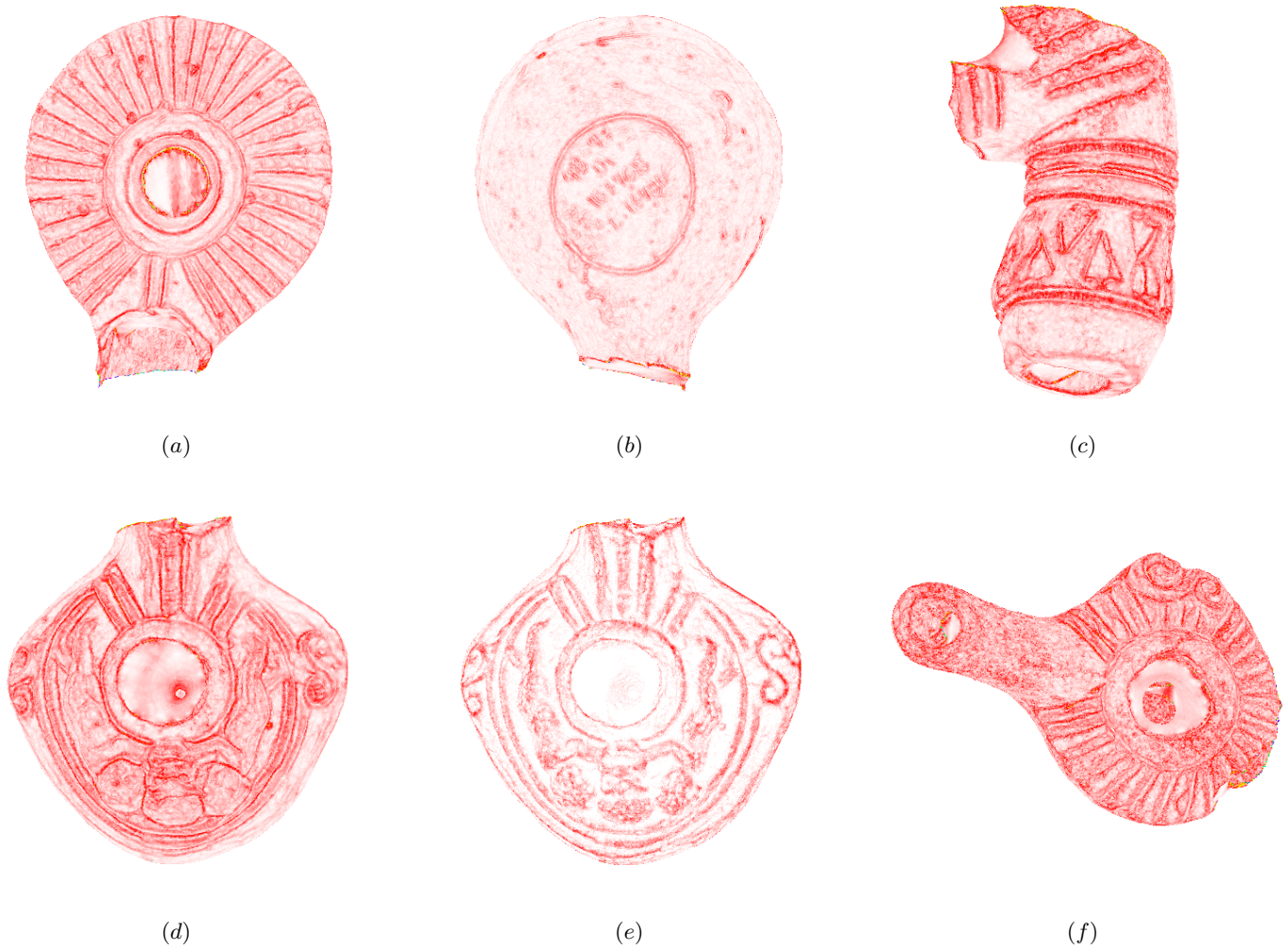

Figure 5: *The horizon measure computed for a number of archeological artifacts. Note that (a) and (b) are the opposite sides of an ancient lamp. Also, (d) and (e) compare the horizon measure and visible horizon measure of another ancient lamp artifact.*

which can have as many as $350,000$ polygons.

Applications: We have applied our horizon measure and visible horizon measure to the visualization of archeological artifacts. Figure 5 shows the rendering using the horizon measure and the visible horizon measure on a number of archeological shapes [Kolomenkin et al. 2008]. Notice that the horizon measures can well capture and present the features in the artifacts. Moreover, the visible horizon measure tends to produce an abstract-style visualization that mimics art (Figures 1 (b), 3 (1b and 2b), and 5 (e)).

Note that we have focused on orientatble surfaces in this paper. Extending this work on non-orientable surfaces is an interesting future direction.

References

COLE, F., GOLOVINSKIY, A., LIMPAECHER, A., BARROS, H. S., FINKELSTEIN, A., FUNKHOUSER, T., AND RUSINKIEWICZ, S. 2012. Where do people draw lines? *Commun. ACM 55*, 1 (Jan.), 107–115.

DECARLO, D., FINKELSTEIN, A., RUSINKIEWICZ, S., AND SANTELLA, A. 2003. Suggestive contours for conveying shape. *ACM Trans. Graph. 22*, 3 (July), 848–855.

HERTZMANN, A., AND ZORIN, D. 2000. Illustrating smooth surfaces. In *Proceedings of the 27th Annual Conference on Computer Graphics and Interactive Techniques*, ACM Press/Addison-Wesley Publishing Co., New York, NY, USA, SIGGRAPH '00, 517–526.

JUDD, T., DURAND, F., AND ADELSON, E. 2007. Apparent ridges for line drawing. *ACM Trans. Graph. 26*, 3 (July).

KOLOMENKIN, M., SHIMSHONI, I., AND TAL, A. 2008. Demarcating curves for shape illustration. *ACM Trans. Graph. 27*, 5, 157.

OHTAKE, Y., BELYAEV, A., AND SEIDEL, H.-P. 2004. Ridge-valley lines on meshes via implicit surface fitting. *ACM TRANS. GRAPH 23*, 609–612.

ZHANG, E., AND TURK, G. 2002. Visibility-guided simplification. In *Proceedings of the Conference on Visualization '02*, IEEE Computer Society, Washington, DC, USA, VIS '02, 267–274.

A Mathematical Background

To facilitate the discussion, we first provide a few useful concepts and results.

Defintion 1. *Given a non-empty subset $U \subset S^2$, the* co-directional set *of U is defined as $Q_U^+ = \{\mathrm{v} \in S^2 \mid \mathrm{v} \cdot \mathrm{w} > 0 \quad \forall \mathrm{w} \in U\}$. Similarly, the* contra-directional set *of U is defined as $Q_U^- = \{\mathrm{v} \in S^2 \mid \mathrm{v} \cdot \mathrm{w} < 0 \quad \forall \mathrm{w} \in U\}$. Finally, the* neutral set *of U is defined as $Q_U^0 = \{\mathrm{v} \in S^2 \mid \exists \mathrm{w} \in U$ such that $\mathrm{v} \cdot \mathrm{w} = 0\}$.*

Figure 2 (right) illustrates the concept of co-directional set, contra-directional set, and the neutral set for a spherical triangle (green). The red band near the equator is the neutral set, which divides the sphere into two spherical triangles (white), one of which contains the original spherical triangle (green).

Given a region $K \subset M \subset R^3$, $Q^+_{\Gamma(K)}$ consists of viewing directions from which K is entirely backward-facing. Consequently, we refer to $Q^+_{\Gamma(K)}$ as the *back-facing view set* of K. Similarly, $Q^-_{\Gamma(K)}$ consists of viewing directions from which K is entirely front-facing. Consequently, we refer to $Q^-_{\Gamma(K)}$ as the *front-facing view set* of K. $Q^0_{\Gamma(K)}$ is precisely the horizon viewer set for K.

We now consider some properties of Q_U^+, Q_U^0, and Q_U^- which are relevant to the computation of the horizon measure.

Lemma 1. *$Q_U^+ \bigcap Q_U^- = \emptyset$. Area($Q_U^+$) = Area($Q_U^-$).*

Lemma 2. *$Q_U^0 = S^2 \setminus (Q_U^+ \cup Q_U^-)$.*

Lemma 3. *Given $U \subset V$, $Q_U^0 \subset Q_V^0$. In contrast, $Q_U^+ \supset Q_V^+$ and $Q_U^- \supset Q_V^-$.*

The proofs to Lemmas 1 through 3 are straightforward from the definitions of Q_U^+, Q_U^0, and Q_U^-. We now consider a spherical line segment.

Lemma 4. *Given $\mathrm{v}_1, \mathrm{v}_2 \in S^2$, let $E = \{\mathrm{v}_1, \mathrm{v}_2\}$ and $E' = \{\frac{(1-t)\mathrm{v}_1 + t\mathrm{v}_2}{\|(1-t)\mathrm{v}_1 + t\mathrm{v}_2\|} \mid t \in [0,1]\}$. Then $Q_E^+ = Q_{E'}^+$, $Q_E^0 = Q_{E'}^0$, and $Q_E^- = Q_{E'}^-$.*

Proof. It suffices to show that $Q_E^+ = Q_{E'}^+$. Since $E \subset E'$, we have $Q_E^+ \supset Q_{E'}^+$ (Lemma 3). Consequently, we only need to show $Q_E^+ \subset Q_{E'}^+$, i.e., for any $w \in Q_E^+$, we must also have $w \in Q_{E'}^+$. Since $w \in Q_E^+$, $w \cdot v_1 > 0$ and $w \cdot v_2 > 0$. Thus, $w \cdot ((1-t)v_1 + tv_2) > 0$ for any $t \in [0,1]$. Consequently, $w \in Q_{E'}^+$. □

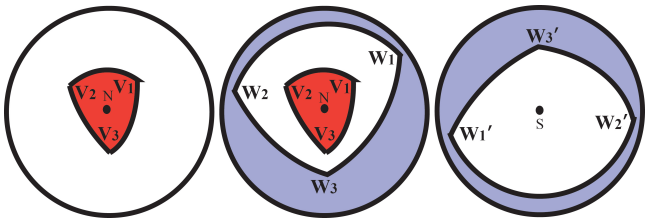

Figure 6: *Given a spherical triangle $\triangle \mathrm{V}_1\mathrm{V}_2\mathrm{V}_3$ in S^2 whose interior covers the north pole (left), the complement of the neutral set with respect to $\triangle \mathrm{V}_1\mathrm{V}_2\mathrm{V}_3$ consists of two disjoint spherical triangles: the co-directional set $\triangle \mathrm{W}_1\mathrm{W}_2\mathrm{W}_3$ and the contra-direction set $\triangle \mathrm{W}_1'\mathrm{W}_2'\mathrm{W}_3'$. The co-directional set is in the northern hemisphere (middle) and contra-directional set is in the southern hemisphere (right).*

Lemma 4 can be extended any set of finite points as follows.

Lemma 5. *Let E be the set of n points $\{\mathrm{v}_1, ..., \mathrm{v}_n\}$ in S^2. Let $E' = \{\frac{\sum_{i=1}^n \alpha_i \mathrm{v}_i}{\|\sum_{i=1}^n \alpha_i \mathrm{v}_i\|} \mid \alpha_i \in [0,1], \sum_{i=1}^N \alpha_i = 1\}$. Then $Q_E^+ = Q_{E'}^+$, $Q_E^0 = Q_{E'}^0$, and $Q_E^- = Q_{E'}^-$.*

The proof to Lemma 5 is similar to that of Lemma 4. In essence, Lemma 5 implies that the co-directional set, the contra-directional set, and the neutral set of any spherical polygon are the same as the spherical convex hull of the polygon. Note that any spherical triangle is convex, i.e., its convex hull is the same as the triangle itself.

With the above results, we are ready to compute the horizon measure of a triangle $\triangle u_1u_2u_3$ in a mesh M. It is straightforward to verify that the set of linearly interpolated normals inside $\triangle u_1u_2u_3$ form a spherical triangle $\triangle \Gamma(u_1)\Gamma(u_2)\Gamma(u_3)$. Recall that the horizon measure of $\triangle u_1u_2u_3$ is the area of the horizon viewer set of $\triangle u_1u_2u_3$, or equivalently, the area of the neutral set of $\triangle \Gamma(u_1)\Gamma(u_2)\Gamma(u_3)$.

Computing the area of neutral set of a spherical triangle $\triangle v_1v_2v_3$ (where $v_i = \Gamma(u_i)$) directly is difficult. Instead, we compute the area of co-directional set of $\triangle v_1v_2v_3$.

Theorem 1. *Given a spherical triangle $\triangle \mathrm{v}_1\mathrm{v}_2\mathrm{v}_3$ which encloses the north pole, $Q^+_{\triangle \mathrm{v}_1\mathrm{v}_2\mathrm{v}_3}$ is a spherical triangle $\triangle \mathrm{w}_1\mathrm{w}_2\mathrm{w}_3$ where $\mathrm{w}_i = \frac{\mathrm{v}_{i-1} \times \mathrm{v}_{i+1}}{\|\mathrm{v}_{i-1} \times \mathrm{v}_{i+1}\|}$ for $i = 1, 2, 3$.*

Proof. Let $\overline{v_{i-1}v_{i+1}}$ be the spherical line segment connecting v_{i-1} and v_{i+1}. Note that $Q^+_{\triangle v_1v_2v_3} = \bigcap_{i=1}^3 Q^+_{\overline{v_{i-1}v_{i+1}}}$ (Lemma 5 and the fact that any spherical triangle is convex). Since the boundary of $Q^+_{\{v_i\}}$ is a great circle in the plane perpendicular to v_i for $1 \le i \le 3$, $Q^+_{\triangle v_1v_2v_3}$ is the spherical triangle bounded by the three aforementioned great circles. The pairwise intersections among the three great circles give the three vertices of $Q^+_{\triangle v_1v_2v_3}$. It is straightforward to verify that the vertices are $w_i = \frac{v_{i-1} \times v_{i+1}}{\|v_{i-1} \times v_{i+1}\|}$. □

Figure 6 illustrates the relationship between a spherical triangle $\triangle v_1v_2v_3$ and its co-directional and contra-directional sets, both of which are also spherical triangles.

Theorem 2. $Q^+_{Q^+_{\triangle \mathrm{v}_1\mathrm{v}_2\mathrm{v}_3}} = \triangle \mathrm{v}_1\mathrm{v}_2\mathrm{v}_3$.

Proof. Denote $Q^+_{\triangle v_1v_2v_3}$ by $\triangle w_1w_2w_3$ where $w_i = \frac{v_{i-1} \times v_{i+1}}{\|v_{i-1} \times v_{i+1}\|}$ for $i = 1, 2, 3$ (Theorem 1). Let $Q^+_{\triangle w_1w_2w_3} = \triangle u_1u_2u_3$.

We have $u_1 = \frac{w_3 \times w_2}{\|w_3 \times w_2\|}$. Recall that $w_2 = \frac{v_1 \times v_3}{\|v_1 \times w_3\|}$ and $w_3 = \frac{v_2 \times v_1}{\|v_2 \times w_1\|}$.

A relevant trigonometric identity states that $(v_1 \times v_3) \times (v_2 \times v_1) = kv_1$ for some constant k. Consequently, $u_1 = v_1$. Similarly, $u_2 = v_2$ and $u_3 = v_3$. □

Theorem 2 states that a spherical triangle $\triangle v_1v_2v_3$ is dual to its co-directional set. This relationship allows us to compute the area of neutral set of $\triangle v_1v_2v_3$ as follows. $Area(Q^+_{\triangle v_1v_2v_3}) = Area(\triangle w_1w_2w_3)$. According to Girard's Theorem, $Area(\triangle w_1w_2w_3) = \sum_{i=1}^3 \theta_i - \pi$ where θ_i is the angle between w_{i-1} and w_{i+1}. Due to the duality between $\triangle w_1w_2w_3$ and $\triangle v_1v_2v_3$, it is straightforward to verify that $\theta_i = \pi - \arccos(v_{i-1} \cdot v_{i+1})$. Consequently, $Area(Q^+_{v_1v_2v_3}) = Area(\triangle w_1w_2w_3) = 2\pi - \sum_{i=1}^3 \arccos(v_{i-1} \cdot v_{i+1})$. Therefore, $Area(Q^0_{v_1v_2v_3}) = 4\pi - 2Area(Q^+_{v_1v_2v_3}) = 2\sum_{i=1}^3 \arccos(v_{i-1} \cdot v_{i+1})$.